Proceedings World Geothermal Congress 2010
Bali, Indonesia, 25-29 April 2010

Discriminating Alteration of Pyroclastic Flow Deposits in an Active Volcano by SAR Image Analysis for Assessing the Geothermal System

Asep Saepuloh and Katsuaki Koike

Graduate School of Science and Technology, Kumamoto University, Kurokami 2-39-1, Kumamoto 860-8555, Japan

saepuloh@gmail.com, koike@gpo.kumamoto-u.ac.jp

Keywords: alteration, image fusion, SAR β^0, Hyperion

ABSTRACT

Field mapping activity for an active volcano mainly in the Torrid Zone is usually hampered by several problems such as steep terrain and bad atmosphere conditions. In this paper we present a simple solution for such problem by analyzing Synthetic Aperture Radar (SAR) and optical sensor image data. By a combination of two types of satellite images, we detected the geothermal paths by identifying the alteration zone termed A-zone. The main purpose of this study is to discriminate alteration of the pyroclastic flow deposits and estimate their alteration degree by selecting Mt. Merapi in central Java, Indonesia, as a study site and targeting the eruptions during May-June 2006. To delineate the A-zone, we applied an image fusion technique using a ratio image of RADARSAT-1 SAR β^0 data and an MNF transformation of Hyperion image data. The acquisition dates of these images were almost the same to reduce large different change in the image characteristics. In addition, a field survey was carried out to check the usefulness of the image fusion results. The A-zone is found to extend in the eastern flanks by 1.5 km^2 which are covered mainly by the old pyroclastic flow deposits. This area can be interpreted as an ascent flow zone of hydrothermal fluids beneath the summit.

1. INTRODUCTION

The Torrid Zone weather conditions, such as heavy rain and thick clouds, prevent the application of optical remote sensing for monitoring and detecting surface materials. Moreover, the ashes and gases from the crater usually cover thickly over the summit of an active volcano. To overcome this problem, we combined two types of satellite images, RADARSAT-1 SAR and Hyperion. The superiority of SAR images owes that they can provide periodic and synchronous earth observations regardless of the time or weather. Mt. Merapi in central Java, Indonesia, was chosen as a study site (Figure 1). This volcano is significant to be investigated for hazard mitigation and geothermal study because of short interval of eruptions with extrusion of large amounts of pyroclastic flows.

Since SAR backscatter is more sensitive to the Earth surface roughness than the rock types (Saepuloh and Koike, 2009), we adopt an image fusion technique, Intensity-Hue-Saturation color transformation, using SAR β^0 and Hyperion image data acquired by the advanced optical sensor with many observation wavelength bands from visible to short-wave infrared regions. We demonstrate that the fusion technique is effective not only to delineate the alteration zone termed A-zone but also to classify the degree of alteration by estimating their surface roughness. One basis of this classification is that the surface of strongly altered rocks is smoother than the fresh rocks in general.

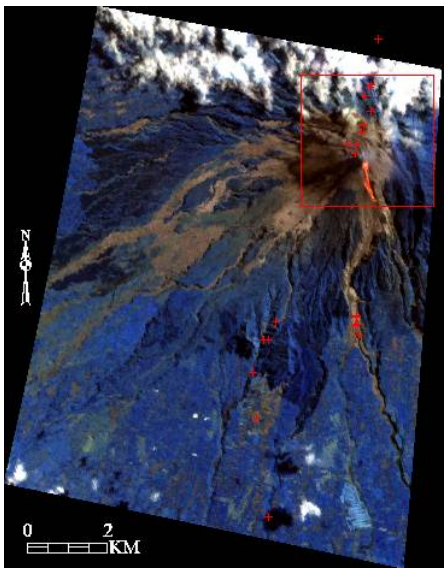

Figure 1: Mt. Merapi on a RGB color composition of a Hyperion image using three bands, 2.19 µm (R), 1.65 µm (G), and 1.07 µm (B). Red rectangular and red "+" stand for the main target area and rock sample locations, respectively.

In addition, rock samples collected by a field survey and their reflectance spectra corresponding to the wavelength bands of Hyperion data were used to check the correctness of the image fusion result. Their reflectance spectra were used as a reference data set for the Hyperion image classification by the Spectral Angle Mapper (SAM). Five endmembers were defined for the different alteration degrees from weakly to strongly altered rocks. By comparing the SAM results with the image fusion result, the alteration rocks were clarified to correspond with the A-zone detected by the image fusion. Therefore, the image fusion technique can be used to mapping the A-zone in a geothermal system which may be caused by the ascent flows of hydrothermal fluids.

2. DATA COLLECTION, PREPARATION, AND METHODOLOGY

There are two types of data used in this study: satellite image data and 16 rock samples collected by field survey in November 2008. The reflectance spectra of the rock samples from visible to short-wave infrared regions were measured by a laboratory spectrometer to identify mineral compositions.

2.1 Data Collection

We used two scenes of RADARSAT-1 SAR with the same off-nadir angle for producing a ratio image of them and one scene of Hyperion data at level 1R. The same off-nadir angle is a suitable condition for the ratio processing to

reduce different geometrical distortion in the images. Acquisition dates of the three scenes are near (within two months) to avoid large change of surface conditions. Details of the data are listed in Table 1.

Table 1: Specification of three scenes of satellite image data used in this study.

Sensor	Orbit Date	Off-nadir	Resolution
RADARSAT-1	May 17, 2006	32.9°	15 m
RADARSAT-1	Jul. 4, 2006	32.9°	15 m
Hyperion	Aug. 11, 2006	0	30 m

We collected the 16 samples mainly along Boyong and Gendol Rivers and around the summit as the sample locations shown in Figure 1. Generally, the rock samples are divided into two types, pyroclastics and lava flows. Another criterion for the classification is three types, old rocks associated with the previous eruptions, new rocks formed after the eruptions in May-June 2006, and altered old rocks. Since Mt. Merapi has erupted repeatedly as a recent volcano, the area of altered rocks is limited near the summit. Figure 2 presents an example of outcrop of the altered rocks containing clay minerals such as kaolinite and montmorilonite that originated from strong alteration of original materials, mainly pyroclastics as discussed in the section 4.

Figure 2: Field photograph of altered rocks in the eastern part from the summit.

2.2 Data Preparation

The two RADARSAT-1 SAR level-0 data were processed using AV-APP 3.0 to generate Single Look Complex (SLC) image. Then, the radar brightness value ($ß^0$) was calculated by the following equation:

$$\beta^0 = 10 * \log_{10}\left[\left(\frac{DNI_j}{A2_j}\right)^2 + \left(\frac{DNQ_j}{A2_j}\right)^2\right] \text{DB} \qquad (1)$$

where DNI_j and DNQ_j are the digital values of the *I* and *Q* components at pixel, *j*, and $A2_j$ is the look-up table (LUT) value. The offset was not used in the SLC generation.

The radar backscatter is affected by three factors, local slope, roughness, and dielectric constant of surface material. The slope factor can be reduced by a ratio operation of two $ß^0$ images, because this factor is common to both images. Since the main volcanic product is pyroclastic flow deposits, the dielectric constant of material may be similar. Therefore the ratio (*RO*) image is only a function of roughness factor at each pixel.

As for the Hyperion image data that was calibrated radiometrically only, we applied an atmospheric correction, Fast Line-of-sight Atmospheric Analysis of Spectral Hypercubes (FLAASH), which is a module of ENVI software, before the image processing. After the processing, geometric correction was adopted to the Hyperion and the *RO* images using an ASTER orthorectified image with 30 m resolution as the reference. All images were co-registered by selecting more than 52 ground control points and by the RMS error for image to image registration smaller than 0.02 pixel.

To deal with many band data of the Hyperion image (196 usable bands out from 242 bands in total), we applied a Minimum Noise Fraction (MNF) transformation by Boardman and Kruse (1994) to select the suitable bands for the image analysis. This transformation can determine the inherent dimensionality of image data to segregate noise in the data and to reduce the computational requirements for subsequent processing by the two rotations. The first rotation uses the principal components of the noise covariance matrix to decorrelate and rescale the noise in the data. The second rotation uses the principal components derived from the original image data after they have been rotated and rescaled by the noise standard deviation. After the MNF transformation, 167 bands were retained as meaningful data. Figure 3 shows the graph of MNF bands and their eigenvalues. The MNF band 1, 2, and 3 components have the three largest eigenvalues and then, we select them for the image fusion with the *RO* image.

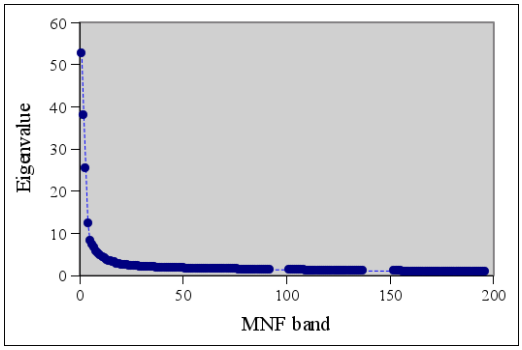

Figure 3: Eigenvalues of Minimum Noise Fraction (MNF) bands selected for image fusion.

2.3 Methodology

The superiority of SAR image is that it can discriminate surface materials by backscattering intensity mainly related to the surface roughness. On the other hand, optical sensor image is precise for identifying surface materials by reflectance characteristics. Therefore, the image fusion of both data type must be more effective to detect the kind of materials and further, their physical characteristics such as particle size, weathering degree, and alteration condition. Our intension of applying the image fusion is to improve characterization of pyroclastic flow deposits.

There are several image fusion methods available that can enhance the features in the images, such as band selection method, color related techniques, and statistical/numerical method (Pohl and van Genderen, 1998). We selected Intensity-Hue-Saturation (*IHS*) color related technique for the *RO* image and MNF-Hyperion data. The complete work flow is depicted in Figure 4.

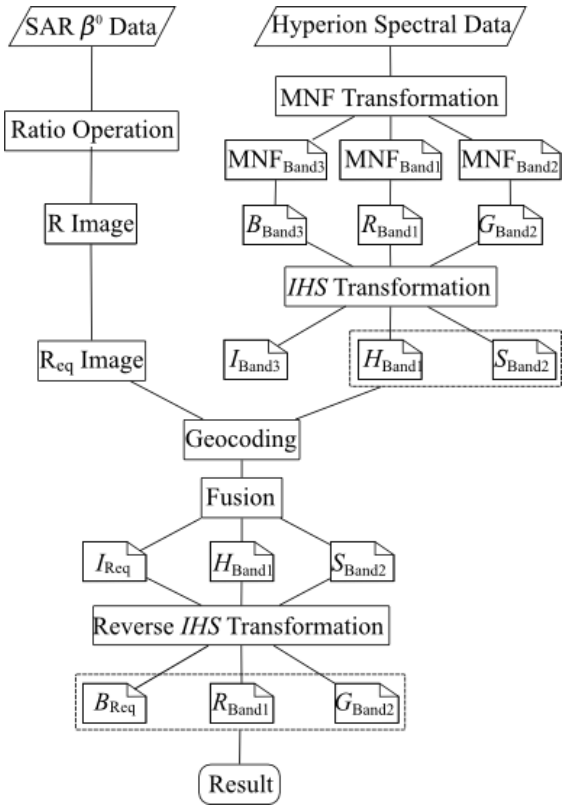

Figure 4: Work flows of image fusion for RADARSAT-1 SAR and Hyperion image data.

At first the MNF 1, 2, and 3 bands are assigned in the *RGB* (Red, Green, and Blue) color space. Then the *RGB* image is used as input for *IHS* transformation by the following equations (Pellemans et al., 1993):

$$I = \frac{1}{\sqrt{3}}(R + G + B) \tag{2}$$

$$H = \tan^{-1}\left(\frac{G - R}{R + G - 2\mathrm{B}}\right) \tag{3}$$

$$S = \sqrt{\frac{1}{6}\left((R + (G - 2\mathrm{B}))^2 + (R - G)^2\right)} \tag{4}$$

where *I*, *H*, *S* stand for Intensity, Hue, Saturation.

Contrast stretching by the histogram equalization is then applied to the *RO* image for standardizing with the MNF band 3 for *I* component (Chen et al., 2003). By this processing, the stretched *RO* image can have similar values of variance and mean as the MNF band 3 as demonstrated in Table 2. Then, the *I* of MNF band 3 is replaced by the *RO* equalized image for the back-transformation into the RGB color space. The advantage of the technique is to enhance the color in the image and increase the Hyperion spatial resolution from 30 m to 15 m. The resultant image is shown in Figure 5.

3. IMAGE FUSION FOR DISCRIMINATING THE A-ZONE

Mt. Merapi is classified as a young active volcano from the geological time scale. The age of Ancient Merapi is only about 40,000 y BP (Camus et al., 2000), which restricts the surface manifestation of geothermal system such as solfatara and fumarole. Only at and around the summit, we can see the solfatara and fumaroles accompanying strongly altered rocks by field-based investigations. Therefore, detection of the surface manifestation of geothermal system and A-zone using the fusion image must be important to clarify the total geothermal system at Mt. Merapi.

Table 2: Mean and variance of MNF band 3 of intensity (*I*) and two *RO* values before and after equalization processing.

	Mean	Variance
$MNF_{intensity}$ (*I*)	0.91	0.07
RO original	1.09	2.47
RO equalization	0.25	0.07

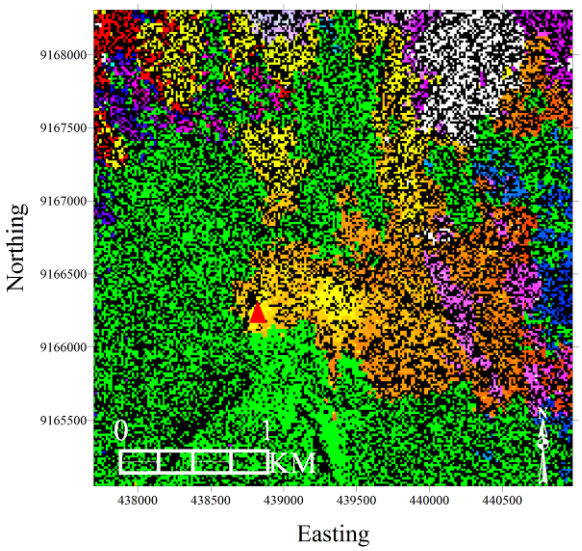

Figure 5: Color composition of image fusion result by R: Hue (MNF band 1), G: Saturation (MNF band 2), and B: Intensity (*RO* equalized value). The A-zone is located in yellow-orange portions in the eastern part from the crater (red triangle).

The fusion image contains noisy-dark pattern which is interpreted to originate from the low values of *RO* equalization. The pattern may express the distribution of materials fragmented from the pyroclastic falls after the eruptions in May-June 2006, because the materials covered almost Mt. Merapi.

Beside the noisy-dark pattern, there are seven distinguishable zones characterized by different color. Base on the field survey, we confirmed that the A-zone was located in the yellow-orange zones. Since we produced a color composition image by assigning MNF band 1, MNF band 2, and *RO* equalized value into *R*, *G*, and *B*, the *B* component represents the degree of the surface roughness of the materials: highly rough and smooth surfaces are colored by blue and yellow, respectively. Therefore, the A-zone colored by orange-yellow is relatively smooth surface and we can correlate the alteration process with the surface roughness. The strong alteration decomposes rocks into soils whose surfaces are much smoother than rocks. As the result, the backscattering intensity related to the *RO* equalized value is decreased. In addition, we interpret that the alteration degree of rock type is stronger at the yellow portion than the orange portion. This alteration may have occurred at the pyroclastic flow deposits.

The remarkable A-zone is mainly located at and around the summit and at the eastern part from the summit, which is opposite to the distributions of the latest volcanic products extending at the southwest from the summit. This feature suggests that the alteration process was occurred strongly on the old pyroclastic flow deposits. To check our interpretation, we measured reflectance spectra of the altered rock samples as a ground truth data.

4. DISCUSSION

The reflectance spectra measured of the rock samples are shown in the Figure 6. We divided the rock samples into five types based on their origins: new pyroclastic flows (NP), old pyroclastic flows (OP), new lava dome (ND), old lava dome (OD), and altered pyroclastic flows (AP).The AP originated mainly from the OP that was located near the summit. An important characteristic is that the spectra of AP and OP show similar trend. The AP has deeper spectral absorption than OP at the wavelength 1.4 and 1.8 µm. High water content in the alteration minerals is one possible cause for the absorption.

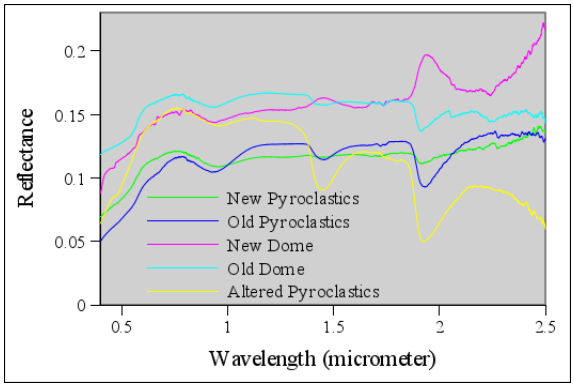

Figure 6: Reflectance spectra of rock samples from visible to short-wave infrared regions.

The strongly altered rock samples of AP are probably rich in kaolinite, montmorilonit, and other silicate minerals. To identify the minerals that characterize the reflectance spectra, the USGS spectral library of alteration minerals (Figure 7) was used. This comparison confirms that the spectra of AP are similar to those of halloysite, kaolinite, montmorilonite, and mordenite. Therefore, the AP rocks are regarded to be composed of these minerals.

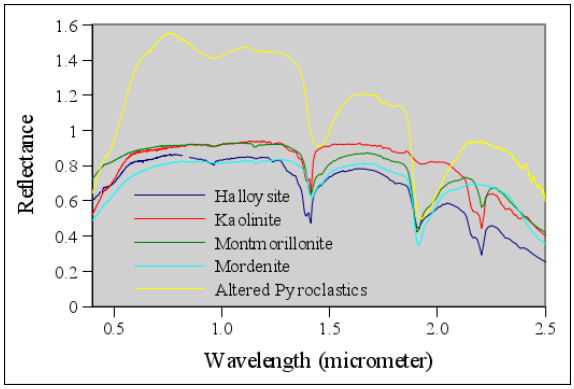

Figure 7: Reflectance spectra of the AP compared with the reference spectra of clay minerals and silicates in the USGS spectral library.

Next, we applied Spectral Angle Mapper (SAM: Kruse et al., 1993) processing for the Hyperion image data to extract the AP distribution. SAM defines the similarity of two spectra by the following angle parameter:

$$\theta = \cos^{-1}\left[\frac{\sum_{i=1}^{n} t_i r_i}{\sqrt{\sum_{i=1}^{n} t_i^2 \sum_{i=1}^{n} r_i^2}}\right] \quad (5)$$

where n is the number of hyper-spectral bands, t is the reflectance of the rock sample spectrum, and r is the reflectance of the reference spectrum.

The reflectance spectra of AP were used as the input endmember of the SAM classification. The smallest angle by the SAM means the highest similarity between the spectra of the reference data and the image data. Here, we assumed the angle less than 0.16 for the criterion of similarity.

The SAM result is depicted in Figure 8 in which the color legend indicated estimation of the alteration degree. This figure highlights that the distribution of altered rocks colored by green correspond precisely with the A-zone detected by the image fusion. It is noteworthy that the yellow portions showing high similarity contain the locations of the strong altered rock samples. Consequently, Figure 8 can be used to estimate roughly the alteration degree at the surface.

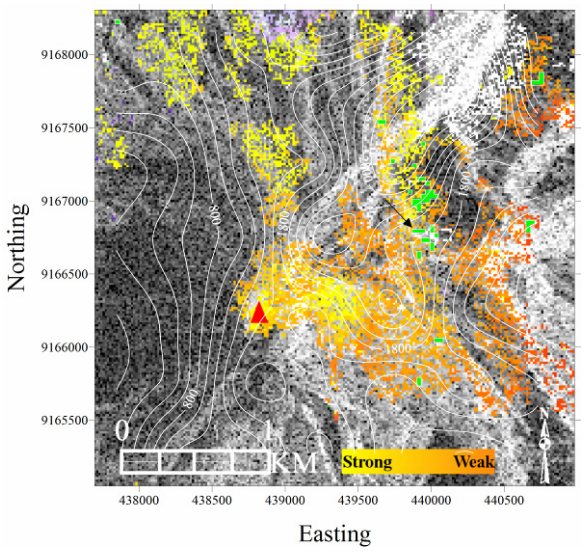

Figure 8: Distribution of the A-zone overlaid with contour lines of lineament density from directional filtering of the SAR $ß^0$ image on July 4, 2006. The black arrow and green polygon stand for the sample location of the AP and the alteration rocks inferred from SAM classification.

To infer the flow paths of geothermal system, we calculated lineament density for each small area from the lineaments extracted using a directional filtering of the SAR β^0 image on July 4, 2006. This filter is designed for four (0°, 45°, 90°, and 315°) azimuths to ensure that the lineaments of all directions can be extracted. The resultant lineament density is overlaid with the A-zone by contour lines in Figure 8, which clarifies that the trends of lineament density agree with the A-zone distribution.

The highest anomaly zones are mostly located at the eastern part near the summit. This zone may be composed of strongly fractured rocks that were caused by uplifting energy of the magma pressure. This interpretation agrees with the location of magma reservoir at the eastern part from the summit (e.g. Beauducel and Cornet, 1999; Tiede et al., 2005).

This reservoir location oblique to the summit may have fractured the rocks chiefly in the eastern part. The fractures can act as flow paths of the hydrothermal system and therefore, the rocks around the paths were altered strongly by the hydrothermal fluids. The A-zone is estimated at about 1.5 km^2 in size and mainly located within the 2-km radius from the summit to the east. It can be concluded that the A-zone expresses the ascent flow zone of the geothermal system and the extent of the flow.

5. CONCLUSION

The capability of SAR image data to specify the A-zone regardless of the weather condition was proved by a combination with hyperspectral optical sensor image data. The roughness degree derived from the SAR backscattering data contributed to estimating the alteration degree of the surface rocks. The strongly altered rocks may correspond with smooth materials which have low bright values in the SAR data.

The spectroscopy analysis confirms that the strongly altered rock samples of the AP are composed by halloysite, kaolinite, montmorilonite, and mordenite. The distributions of the AP inferred from SAM classification correspond precisely with the strong alteration location in the A-zone detected by the image fusion.

The A-zone was mainly detected near the summit with 1.5 km^2 in the area size. By the comparison with the lineament density map, this zone was confirmed to have relations with the pattern of the fractured zone and the magma reservoir location. Therefore we interpreted that the A-zone is an ascent flow zone of the geothermal system at Mt. Merapi because the location is close to the summit.

REFERENCES

Beauducel F, Cornet F.H.: Collection and three-dimensional modelling of GPS and tilt data at MerapiVolcano, Java. Journal of Geophysical Research, 104, (1999).

Boardman, J.W., Kruse, F.A.: Automated spectral analysis: a geological example using AVIRIS data, north Grapevine Mountains, Nevada, Proceedings, ERIM Tenth Thematic Conference on Geologic Remote Sensing, Environmental Research Institute of Michigan, Ann Arbor (1994).

Camus G, Gourgaud A, Mossand-Berthommier P.C., Vincent P.M.: Merapi (Central Java, Indonesia): An outline of the structural and magmatological evolution, with a special emphasis to the major pyroclastic events, Journal of Volcanology and Geothermal Research, 100, (2000), 139–163.

Chen, C.M., Hepner, G.F., Forster, R.R.: Fusion of Hyperspectral and Radar Data using the IHS Transformation to Enhance Urban Surface Features, ISPRS Journal of Photogrammetry & Remote Sensing, 58, (2003), 19-30.

Kruse F., Lefkoff A., Boardman J., Heidebrecht K., Shapiro A., Barloon P., Goetz A.: The spectral image processing system (SIPS) - interactive visualization and analysis of imaging spectrometer data,.Remote Sensing of Environment, 44, (1993), 145-163.

Pellemans, A.H., Jordans, R.W., Allewijn, R.: Merging Multispectral and Panchromatic Spot Images with Respect to The Radiometric Properties of The Sensor, Photogrammetric Engineering and Remote Sensing, 59, (1993), 81-87.

Pohl, C., van Genderen, J. L.: Multisensor image Fusion in Remote Sensing: Concepts, Methods and Applications, Int. J. Remote Sensing, 19, (1998), 823-854.

Tiede C, Camacho A.C., Gerstenecker C, Fernández J, Suyanto I: Modeling the density at Merapi volcano area, Indonesia, via the inverse gravimetric problem. Geochemistry Geophysics Geosystems, 6, (2005), 1-13.

Saepuloh A., Koike K.: Detailed Mapping of Pyroclastic Flow Deposits by SAR data processing for an Active Volcano in the Torrid Zone, Proceedings, International Conference on Earth and Space Sciences and Engineering, Tokyo, Japan (2009).